nature research

https://doi.org/10.1038/s41593-020-00758-5

Supplementary information

Olfactory transmucosal SARS-CoV-2 invasion as a port of central nervous system entry in individuals with COVID-19

In the format provided by the authors and unedited

Supplementary Material for

Olfactory transmucosal SARS-CoV-2 invasion as a port of central nervous system entry in individuals with COVID-19

Jenny Meinhardt[1,§], Josefine Radke[1,2,3,§], Carsten Dittmayer[1,§], Jonas Franz[4,5,6] , Carolina Thomas[4,6], Ronja Mothes[1], Michael Laue[7], Julia Schneider[8], Sebastian Brünink[8], Selina Greuel[9], Malte Lehmann[10], Olga Hassan[1], Tom Aschman [1], Elisa Schumann[1,3], Robert Lorenz Chua[11], Christian Conrad[11], Roland Eils[11,12], Werner Stenzel[1], Marc Windgassen[13], Larissa Rößler[13], Hans-Hilmar Goebel[1], Hans R. Gelderblom[7], Hubert Martin[1], Andreas Nitsche[7], Walter J. Schulz-Schaeffer[14], Samy Hakroush[15], Martin S. Winkler[16], Björn Tampe[17], Franziska Scheibe[18,19], Péter Körtvélyessy[18,20], Dirk Reinhold[21], Britta Siegmund[10], Anja A. Kühl[22], Sefer Elezkurtaj[9], David Horst[9], Lars Oesterhelweg[13], Michael Tsokos[13], Barbara Ingold-Heppner[23], Christine Stadelmann[4], Christian Drosten[8], Victor Max Corman[8], Helena Radbruch[1,#], Frank L. Heppner[1,2,24,#,*]

*Correspondence to: frank.heppner@charite.de

This file includes:

Figs. S1 to S6
Table 1 and 2

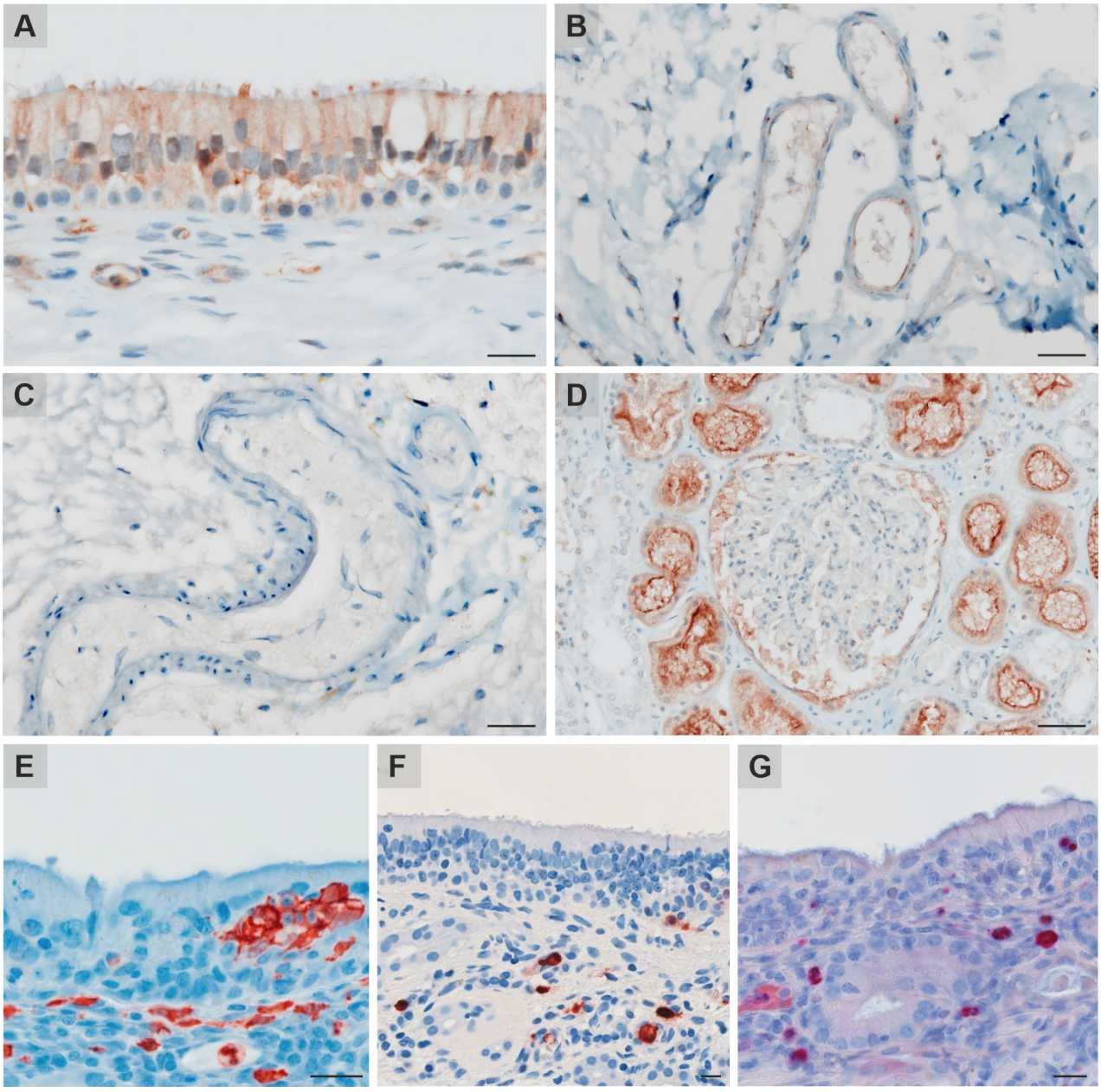

Supplementary Figure 1: ACE 2 and MRP14 immunohistochemical stainings

Immunohistochemical stainings for human ACE2 protein in the olfactory mucosa, CNS and kidney (A –D). A weak reactivity in most of the epithelial cells of the olfactory mucosa can be detected, while neuronal cells were not found to show ACE2 expression (A, brown color, patient no. 15). The endothelium of the olfactory bulb (B, patient no. 26) and CNS tissue from the medulla oblongata (C, patient no. 26) exhibited only weak ACE2 signals. High ACE2

expression was observed in renal proximal tubules, which served as positive control (D, brown, patient no. 8).

Small clusters of infiltrating early activated macrophages and granulocytes (MRP14, red color) in the olfactory epithelium upon SARS-CoV-2 infection (E, patient no. 27). Immunohistochemical staining of the olfactory mucosa from a non-COVID-19 patient shows absence of MRP14 expressing cells in the olfactory mucosa (F, Control No. 6). Only few MRP14-positive cells can be detected in the submucosa. MRP14 is expressed by early activated macrophages and also by granulocytes. To differentiate macrophages and granulocytes in the MRP14 staining, we performed enzymatic chloroacetate esterase staining on serial sections of the MRP14 -stained tissue. This revealed only single granulocytes in the olfactory mucosa (G, red color, patient no. 15) corroborating our interpretation that the majority of MRP14-expressing cells in COVID-19 patients (E) are early activated intramucosal macrophages. Scale bars: A: 20 µm, B: 20 µm, C: 30 µm, D: 80 µm, E-G: 20 µm.

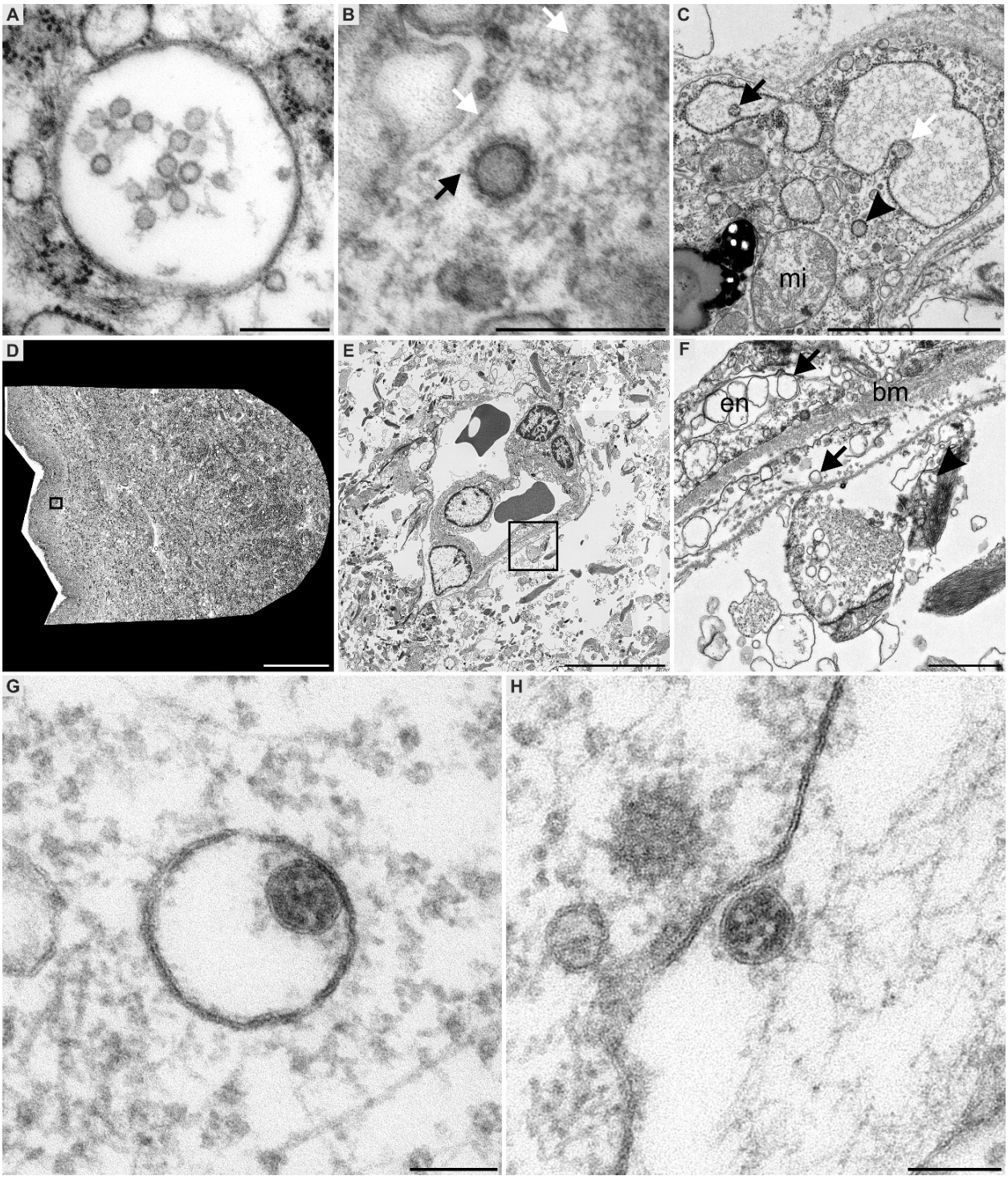

Supplementary Figure 2: Morphological mimics and autolysis as ultrastructural pitfalls in coronavirus identification in autopsy tissues and SARS-CoV-2 ultrastructural presentation under cell culture conditions

SARS-CoV-2 PCR-positive COVID-19 lung autopsy samples (A – C; A+B: Patient No. 6; C: Patient No. 7) and medulla oblongata (D – F; patient 6) with low numbers of RNA copies. Subcellular structures such as multi-vesicular bodies (MVBs; A) and coated vesicles (B) are easily mistaken as coronaviruses. However, in contrast to coronavirus, MVBs lack characteristic substructure represented by electron dense ribonucleoprotein (RNP) and delicate surface projections. Additionally, size and position of the vesicles are different in coronavirus, e.g. coated vesicles (B) are not inside a membrane compartment (note the cytoplasmic microtubules indicated by white arrows), lack the substructure, and show too pronounced and regular surface projections (black arrow). Invaginations (C, white arrow) of e.g. rough endoplasmic reticulum cisternae (rER, pneumocyte) may also mimic coronavirus in some cross-sectional orientations (compare to vesicular structure; black arrow), due to high electron density and granular appearance of ribosomes, resembling RNP; note cytoplasmic vesicle, most likely of the rER, with granular appearance (C, arrowhead). Large-scale digitization of the entire ultrathin section of post-mortem medulla oblongata tissue (D - F) at a pixel size of 4 nm. (E) and (F) showing digitally magnified areas of the insets in (D) and (E), demonstrating post-mortem-related changes e.g. vacuolation (E - F, arrows in F), swollen mitochondria (arrowhead in F) blurring coronavirus detection compared to freshly prepared human or laboratory animal specimens or cell culture. Ultrastructure of SARS-CoV-2 (isolate Italy-INMI1) virus particles in Vero E6 cells (G, H: 24 h post infection) demonstrate the intracellular localization within a membrane compartment (G) with a typical attachment to the inner membrane surface. Note the preservation of surface projections which is due to the application of an bloc-staining (tannic acid and uranyl acetate)[50]. Electron dense material, likely representing RNP, can be detected in the particle interior, partly also directly underneath the envelope membrane. Extracellular coronavirus particle with similar structural appearance than the intracellular particle is attached to the apical plasma membrane (H). Scale bars: A, B: 250 nm; C: 2000 nm; D: 250 µm; E: 10 µm; F: 1000 µm; G, H: 100 nm.

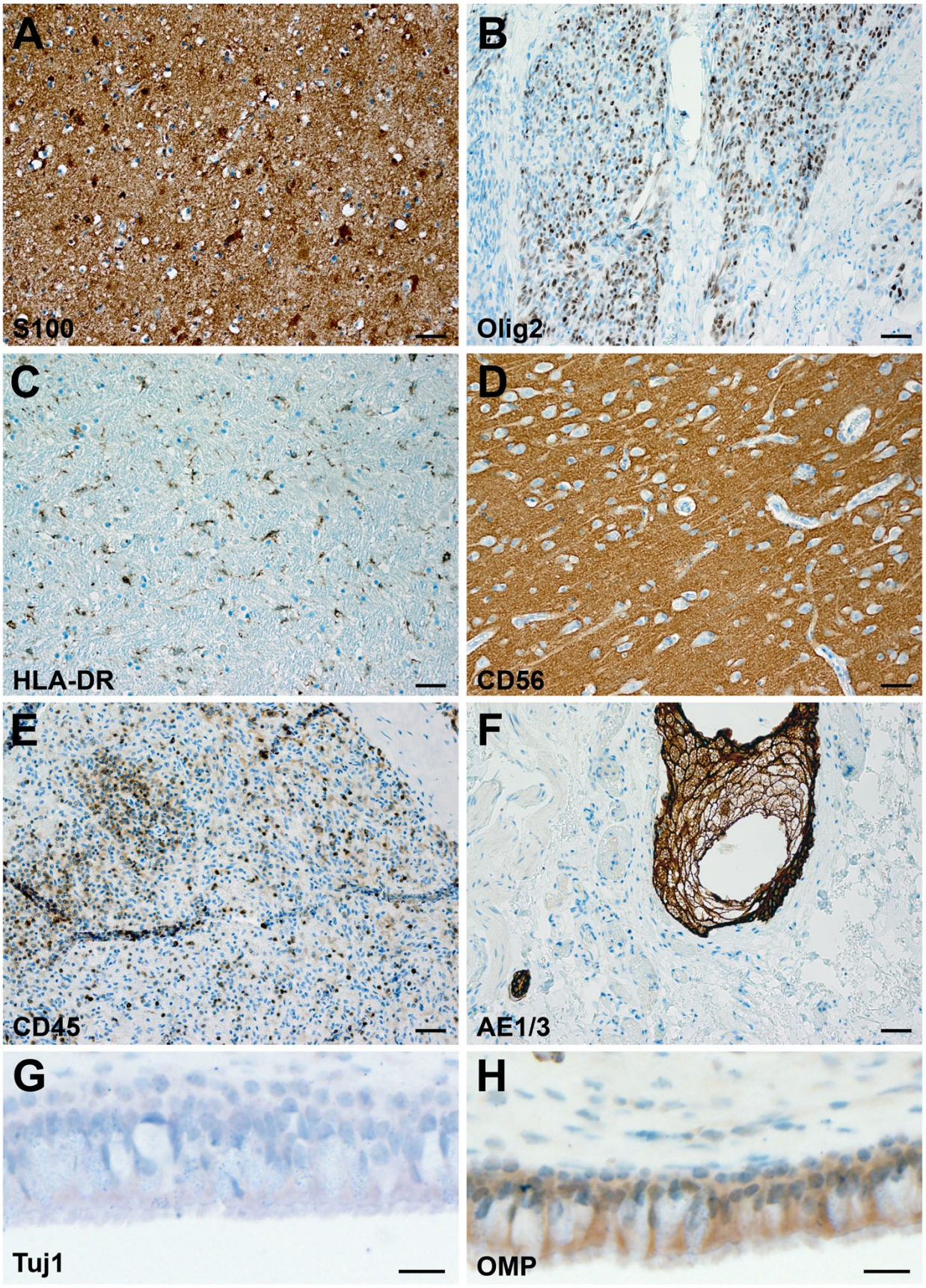
A
S100
B
Olig2
C
HLA-DR
D
CD56
E
CD45
F
AE1/3
G
Tuj1
H
OMP

Supplementary Figure 3: Immunohistochemical control stainings

To biologically validate all immunohistological stainings, control tissues with known expression pattern harboring or lacking the expected antigens were used. A positive immunoreactivity is illustrated by brown color. Immunohistochemical staining for S100 protein within normal (non-diseased) autopsy brain tissue depicts glial cells such as astrocytes and neurons, while endothelial cells are spared (A). (B) illustrated the positive control tissue for Olig2, which is known to show nuclear immunoreactivity in glioma tumor cells, while endothelial cells are not reactive to Olig2. HLA-DR immunoreactivity in the brain even under non-pathologic conditions is typically found on CNS-intrinsic myeloid cells, namely microglia, while e.g. neural/neuronal cells show no positivity for HLA-DR (C). All neuroepithelial cells in the CNS demonstrate a strong immunoreactivity for CD56, which cannot be found on endothelial cells (D). Tonsils were used to serve as positive control tissue for the general leukocyte marker CD45, while connective tissue of the capsula is not stained (E). The epithelium in a non-diseased skin sample in (F) shows strong immunoreactivity for the pan-cytokeratin marker AE1/3 in contrast to the surrounding connective tissue. The nasal respiratory mucosa of a non-COVID-19 autopsy case – in contrast to the olfactory mucosa - lacks $Tuj1^{+}$ (G) and OMP^{+} (H) neural/neuronal cells; the diffuse brown color in H only depicts unspecific background color compared to the specific OMP-signal shown in Fig. 2G resembling olfactory mucosa. Scale bars 1-F 50 µm; G,H: 20 µm

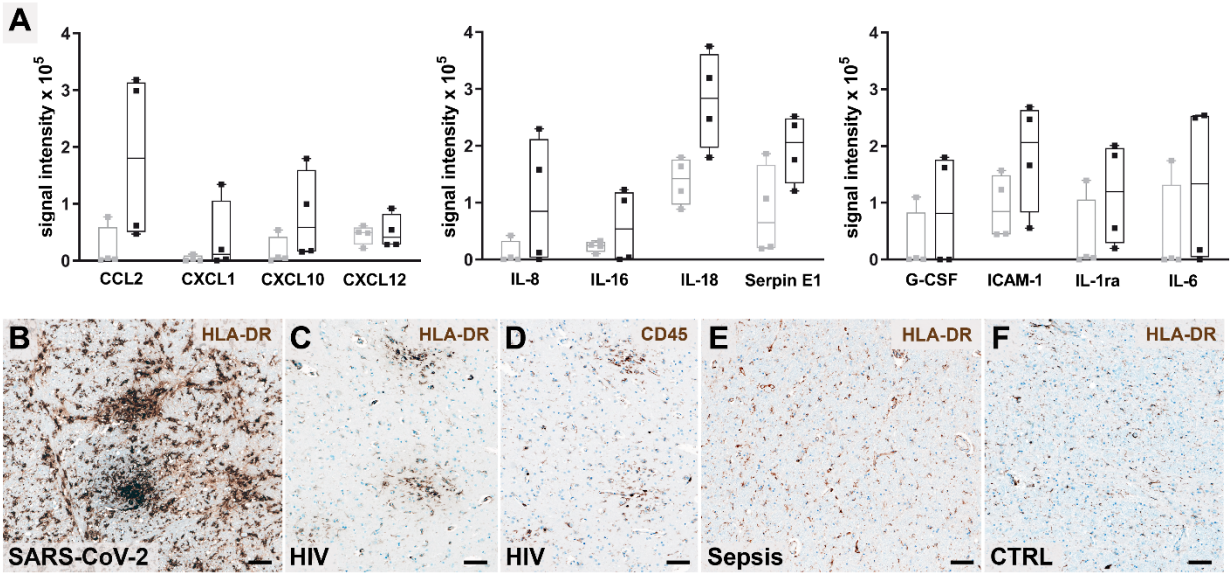

Supplementary Figure 4: Inflammatory imprint of CSF and CNS tissue in COVID-19 patients

CSF levels of detectable inflammatory proteins of four COVID-19 autopsy cases (black, n=4 patients (patient no. 7, 9, 12 and 16) tested once) and four non-COVID-19 control cases (grey, n=4 patients (control no. 1 – 4) tested once) based on a semi-quantitative analysis (A). Due to the semiquantitative nature of the data and access to only a limited number and amount of CSF samples no detailed statistical analysis could be performed. Box plots show individual data points, median (centerline), 25th and 75th percentiles (box), and range (whiskers).

Correspondingly, representative histological analyses of HLA-DR- and CD45-stained tissues of COVID-19 and non-COVID-19 control cases (B-F) revealed a prominent HLA-DR upregulation on cells resembling microglia/macrophages and identified distinct microglia nodules in the medulla oblongata of COVID-19 cases, while there were no gross inflammatory leukocytic infiltrates detectable (N=13 from 25 analyzed patients; see also table 2; patient no. 16). CNS tissue from an encephalitis case due to cerebral HIV infection (C, D) was used as positive control illustrating HLA-DR-positive microglia nodules (C) and CD45-positive leukocytic infiltrates (D) in the medulla oblongata (control no. 12). HLA-DR upregulation is also detectable in the medulla oblongata in septic patients (E, control no. 13) in contrast to CNS tissue derived from ALS subjects (F, control no. 2). Scale bars (B-F): 100 µm

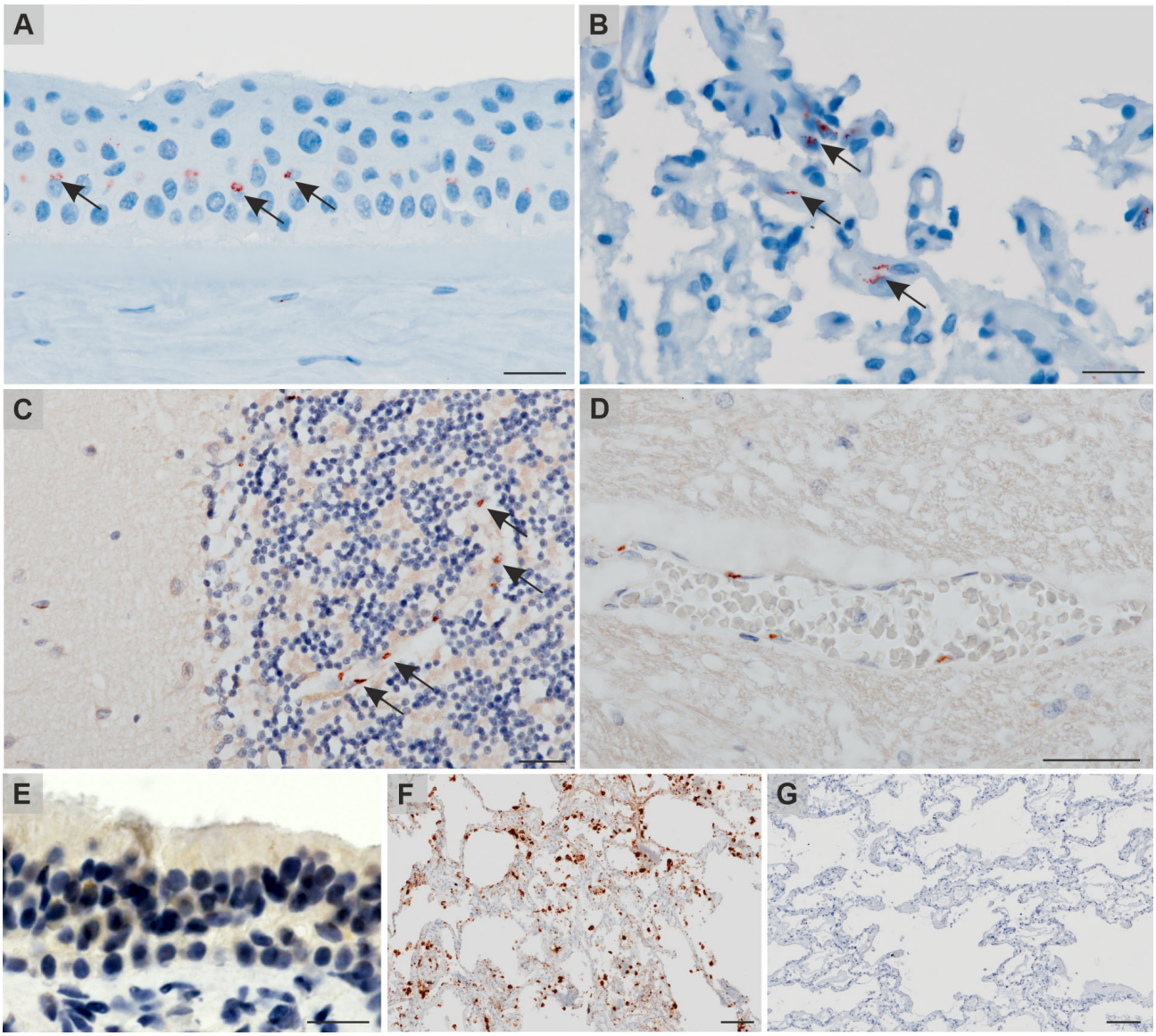

Supplementary Figure 5: SARS-CoV S Immunohistochemistry and *in-situ* hybridization

SARS-CoV spike protein (SARS-CoV S) was detectable in the cornea (A, red color, arrows, patient no. 22, N=1 out of 1) and in endothelial cells of small CNS vessels within the olfactory bulb (B, red color, arrows, patient no. 4; N=1 out of 1) as well as in the cerebellum (C, brown color, arrows, patient no. 20; N=2 out of 3). A representative image of identically stained CNS tissue from a non-COVID-19 autopsy case shows only faint perinuclear immunoreactivity for SARS-CoV in the endothelial cells of small CNS vessels within the medulla oblongata (D, brown color, control no. 7; N=1 out of 4 stained control cases), while the olfactory mucosa from a non-COVID-19 patient displayed no SARS-CoV S signal (E, control no. 6; N=4 out of 4 stained control

patients).Similarly, SARS-CoV RNA *in situ* hybridization (ISH) demonstrated an intense signal in lung tissue of a SARS-CoV-2 positive patient (F, brown color, patient no. 3; N=2 out of 2), while there was no signal in lung tissue taken from a control autopsy case without COVID-19 (G, control no. 5; N=1 out of 1). Scale bars: A, B, C: 25 µm, D: 100 µm, E-G: 25 µm.

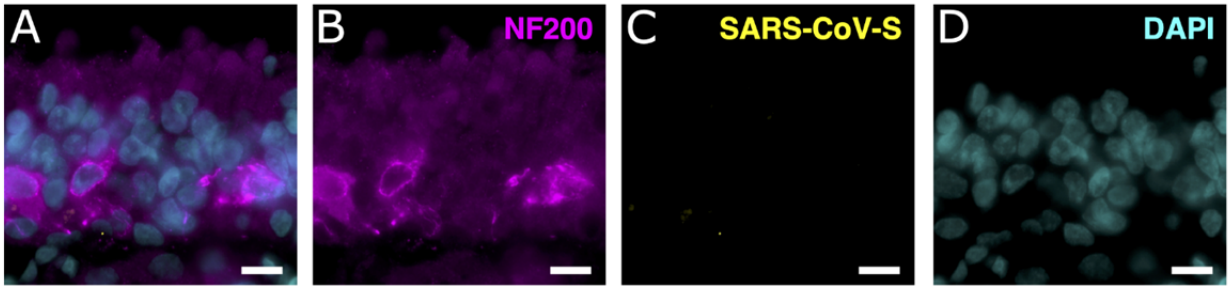

Supplementary Figure 6: Immunofluorescence of SARS-CoV Spike protein (S) in the olfactory mucosa

Olfactory mucosae derived from two distinct non-COVID-19 autopsy control cases were stained for SARS-CoV Spike protein (S) and NF200 or Tuj1 (N=2 from 2; control no. 6, control no. 8). Representative epifluorescent microscopic images of olfactory mucosae derived from non-COVID-19 autopsy control cases – as opposed to those of COVID-19 cases shown in Fig. 4C, G, K - revealed no intracytoplasmic SARS-CoV S within NF200+ OSNs (Tuj1 is not shown). NF200 (magenta; Alexa 488) depicts cells of neuronal origin, SARS-CoV S (yellow, Alexa 555) visualizes the lack of presence of SARS-CoV, DAPI (D; petrol) identifies all cell nuclei (N=1; control patient no. 8). Each channel (B-D) is displayed separately. Scale bars: A-D 10 µm.

Supplementary Table 1

Case	Gender	Age [years]	SARS-Cov-2 qPCR ante-mortem	Duration of illness [days]	Pre-existing Conditions / Concomitant Diseases					
					Cardiovascular	Respiratory	Gastrointestinal	Urinary	Cerebral	Miscellaneous
P1	M	71	Positive	28	Arterial hypertension	Bronchial asthma	-	-	-	-
P2	F	79	Positive	14	Arterial hypertension, coronary heart disease	-	-	Stage 3 chronic kidney disease	Dementia	Obstructive sleep apnoea
P3	F	90	Positive	12	Arterial hypertension, coronary heart disease, atrial fibrillation	COPD, stage 2 (Gold classification)	Liver cirrhosis	Stage 3 chronic kidney disease	-	-
P4	M	79	Positive	25	-	-	-	-	-	Right hemiplegia since childhood
P5	F	79	Positive	20	Arterial hypertension, coronary heart disease	-	-	-	Left middle cerebral artery stroke, right hemiataxia (2019)	Type 2 diabetes mellitus, Osteoporosis, Hyperlipidemia
P6	M	68	Positive	34	-	-	-	-	-	-
P7	M	61	Positive	19	Arterial hypertension, coronary heart disease	Heavy smoker	Cholecystectomy	-	-	Class 1 Obesity
P8	F	68	Positive	34	Arterial hypertension, coronary heart disease	COPD, stage 2 (Gold classification)	-	-	-	Class 1 Obesity, Hypothyroidism
P9	M	76	Positive	14	Arterial hypertension, ischemic cardiomyopathy, myocardial infarction (2008)	Heavy smoker	-	-	-	-
P10	F	56	Positive	27	Arterial hypertension	-	-	-	-	Type 2 diabetes mellitus, Class 1 obesity, breast cancer (2007)
P11	M	92	Positive	29	Intermittent atrial fibrillation	-	-	-	Dementia	-
P12	F	67	Positive	24	Arterial hypertension	-	Sigma diverticulosis	-	Right frontal intracerebral hemorrhage with infarction (2009), left-sided hemiparesis, VP-Shunt (2010)	Rheumatoid arthritis
P13	M	62	Positive	31	Arterial hypertension	Heavy smoker	-	-	Vascular dementia, left-sided watershed stroke (2016), right-sided hemiparesis	Hyperlipo-proteinemia
P14	F	78	n.d., clinical presentation suggestive of COVID-19	N/A	Arterial hypertension, atrial fibrillation, aortic/mitral valve insufficiency	Small cell lung cancer	-	-	-	-
P15	M	81	Positive	11	Arterial hypertension, atrial fibrillation, abdominal aortic aneurysm	-	-	-	Ischemic stroke with left-sided hemiparesis	Type 2 diabetes mellitus, osteoporosis, hyperthyroidism
P16	M	74	Positive	51	Arterial hypertension	-	-	Nephrolithiasis	-	Class 2 obesity
P17	M	70	Positive	51	-	-	-	Bladder cancer (1999; treated curatively)	-	-
P18	F	30	n.d., clinical presentation suggestive of COVID-19	21	-	CMV reactivation + toxoplasmosis with pulmonary involvement	Intestinal acute graft versus host disease (GvHD)	-	Cerebral toxoplasmosis	Allogenic stem cell transplantation (2019), Ewing sarcoma (2013)
P19	M	77	Positive	51	Arterial hypertension	Pulmonary emphysema	-	-	-	-
P20	M	57	Positive	59	-	-	-	-	-	-
P21	M	79	Positive	N/A	-	Heavy smoker	Hepatic steatosis, cholelithiasis	Kidney cysts	-	Psoriasis, gonarthrosis

Case	Gender	Age [years]	SARS-Cov-2 qPCR ante-mortem	Duration of illness [days]	Pre-existing Conditions / Concomitant Diseases					
					Cardiovascular	Respiratory	Gastrointestinal	Urinary	Cerebral	Miscellaneous
P22	M	69	Positive	49	Arterial hypertension	-	-	-	-	Polyneuropathy, alcohol abuse (abstinence for 18 years)
P23	M	89	Positive	14	Arterial hypertension, arteriosclerosis	-	Cholelithiasis	-	Vascular dementia	Type 2 diabetes mellitus, polyneuropathy, benign prostatic hyperplasia
P24	M	74	Positive	35	Coronary heart disease, severe aortic valve stenosis, biologic aortic valve prothesis	-	-	-	-	-
P25	M	72	Positive	79	Arterial hypertension	-	-	-	-	Class 2 obesity, Obstructive sleep apnoea
P26	F	45	Positive	19	Arterial hypertension	Bronchial asthma	-	-	-	Alcohol abuse
P27	M	71	Positive	N/A	-	-	-	-	Parkinson's disease	-
P28	M	80	Positive	30	Arterial hypertension, atrial fibrillation, endocarditis (2014)	-	-	Stage 4 chronic kidney disease	-	Granulomatosis with polyangiitis, anemia, polyneuropathy, osteoporosis
P29	F	72	Positive	N/A	-	-	-	-	-	-
P30	F	98	Positive	4	Arterial hypertension, atrial fibrillation, bradycardia	-	-	-	Left middle cerebral artery stroke	-
P31	M	68	Positive	35	-	-	-	-	-	-
P32	M	68	Positive	58	Arterial hypertension, atrial fibrillation, coronary heart disease, myocardial infarction	COPD	Acute pancreatitis	Stage 2 chronic kidney disease	Basilaris thrombosis with mechanical thrombectomy	Bullous pemphigoid, type 2 diabetes mellitus
P33	M	63	Positive	29	Bradycardiac atrial fibrillation	-	Barrett's esophagus	-	Early onset dementia (2013)	Cachexia
C1	F	63	n.d.	N/A	-	-	-	-	Amyotrophic lateral sclerosis	-
C2	F	62	n.d.	N/A	-	-	-	-	Amyotrophic lateral sclerosis	Cachexia
C3	F	84	n.d.	N/A	Arterial hypertension, coronary heart disease			Stage 1 chronic kidney disease	Amyotrophic lateral sclerosis, unknown neurodenerative disease with dementia	Hypothyroidism, depression, osteoporosis, malnutrition, hypoproteinemia
C4	M	76	n.d.	N/A	-	Pulmonary artery embolism	-	-	Amyotrophic lateral sclerosis	-
C5	M	81	Negative	N/A	Arteriosclerosis	Bacterial pneumonia, diffuse alveolar damage	-	-	Pontine infarction	Type 2 diabetes mellitus
C6	F	45	Negative	N/A	-	Multiple mediastinal and pulmonary lymph node metastases	Untreated poorly differentiated HCC	Stage 2 acute kidney disease	-	Ovarian mass
C7	F	86	n.d.	N/A	-	-	-	-	Amyotrophic lateral sclerosis	-
C8	M	61	Negative	N/A	-	Community-acquired pneumonia, Influenza negative	-	-	Alzheimer's disease	-
C9	F	78	Negativ	N/A	Three-vessel disease, subacute myocardial infarction, paroxysmal atrial fibrillation, carotid arteery disease, arterial hypertension	COPD, heavy smoker		Stage 3 chronic kidney disease	Subcortical left occipito-parietal embolic infarct, early-stage dementia	Oral anticoagulation (Apixaban), hypothyroidism, hypercholesterolemia, , osteoporosis
C10	F	68	Negativ	N/A	-	-	-	-	Prolactinoma	Biopsy tissue

Case	Gender	Age [years]	SARS-Cov-2 qPCR ante-mortem	Duration of illness [days]	Pre-existing Conditions / Concomitant Diseases					
					Cardiovascular	Respiratory	Gastrointestinal	Urinary	Cerebral	Miscellaneous
C11	F	27	n.d.	N/A	-	-	-	-	-	Osteoid osteoma (Frontal sinus) - Biopsy tissue
C12	M	39	n.d.	N/A	-	Pneumonia	-	-	HIV-Encephalitis	HIV (untreated)
C13	F	58	n.d.	N/A	-	-	Cholangitis, metastatic pancreatic cancer	-	-	Septic cholangitis

n.d.= not documented N/A= not available

Supplementary Table 2

Case	Gender	Age [years]	PMI [hours]	Duration of illness [days]	Mechanical ventilation	Neurological alterations during COVID-19 infection	CNS findings					log_{10}SARS-COV-2-RNA copies/10.000 cells											
							Histopathological	SARS-CoV S protein immunohistochemistry / Immunofluorescence (SARS CoV S protein/Tuj1)	ISH	Microglia activation/ - nodules	CD45	Carotis	Cornea	Conjunctiva	Optic nerve	Uvula	Olfactory mucosa	Olfactory bulb	Olfactory tract	Olfactory tubercle	Trigeminal ganglion	Medulla oblongata	Cerebellum
P1	M	71	112	28	✓	Headache	Actue hypoxia in frontal medial gyrus, microglia nodules in medulla, microbleedings in Area prepiriformis and Pons	No IR for SARS-CoV S protein	No signal	**+/+**	-	N/A	N/A	N/A	N/A	N/A	2,01	0	N/A	0	N/A	0	N/A
P2	F	79	148	14	✓	n.d.	Without significant microscopic structural changes	IR for SARS-Cov S protein in endothelial cells in the medulla oblongata	N/A	**+/+**	-	N/A	N/A	N/A	N/A	1,84	5*	3,26	N/A	N/A	N/A	0	N/A
P3	F	90	106	12	♦	Disorientation	Without significant microscopic structural changes	IR for SARS-Cov S protein in endothelial cells in the olfactory bulb and medulla oblongata	No signal	**+/+**	-	N/A	N/A	N/A	N/A	3,22	7,5*	3,1	N/A	N/A	0	1,21	N/A
P4	M	79	56	25	✓	n.d.	Acute pontine infarction	IR for SARS-CoV S protein in the infarct area	No signal	**+/+**	-	N/A	N/A	N/A	N/A	0	0	0	N/A	N/A	0	0	0
P5	F	79	64	20	♦	Transient ischemic attack with disorientation and dysarthria	Acute infarction of the medulla oblongata, cerebral microangiopathy, old right-sided striatocapsular infarct	IR for SARS-Cov S protein in endothelial cells in the medulla oblongata	No signal	**+/-**	-	N/A	N/A	N/A	N/A	0	0	0	N/A	N/A	0	2,74	0
P6	M	68	30	34	✓	Somnolence, rhabdomyolysis, critical illness polyneuropathy	Acute basal ganglia infarct	No IR for SARS-CoV S protein	No signal	**-**	-	N/A	N/A	N/A	N/A	0	3,29	0	N/A	N/A	1,67	2,03	0
P7	M	61	10	19	✓	n.d.	Without significant microscopic structural changes	No IR for SARS-CoV S protein	N/A	**+/-**	-	N/A	N/A	N/A	N/A	0	0	0	N/A	N/A	0	0	0
P8	F	68	16	34	✓	n.d.	Without significant microscopic structural changes	n.d.	N/A	**-**	-	N/A	2,42	0	N/A	0	2,39	0	N/A	N/A	0	0	0
P9	M	76	30	14	♦	N/A	Without significant microscopic structural changes	No IR for SARS-CoV S protein	Positive signal in mucosal cells	**-**	-	N/A	0	0	N/A	1,29	5,6*	0	N/A	N/A	2,05	0	0
P10	F	56	38	27	✓	n.d.	Without significant microscopic structural changes	IR for SARS-CoV S protein in endothelial cells in the cerebellum	No signal	**-**	-	0	N/A	0	N/A	0	0	0	N/A	N/A	0	0	1,94
P11	M	92	72	29	♦	Behavioral changes	Without significant microscopic structural changes	No IR for SARS-CoV S protein	N/A	**+/+**	-	N/A	N/A	0	N/A	0	0	N/A	N/A	N/A	0	1,46	0
P12	F	67	48	24	✓	Intraventricular hemorrhage	Acute infarction of the corpus callosum, chronic leptomeningitis, old right middle cerebral artery infarct with wallerian degeneration reaching to the cerebral crus	No IR for SARS-CoV S protein	N/A	**+/-**	-	0	N/A	0	N/A	N/A	N/A	0	N/A	N/A	0	0	0
P13	M	62	144	31	✓	n.d.	Old left-sided watershed stroke between anterior and middle cerebral artery, old right-sided occipital infarction	N/A	N/A	**+/-**	-	N/A	0	0	N/A	0	1,32	0	N/A	N/A	0	0	0
P14	F	78	192	N/A	♦	N/A	Without significant macroscopic changes	n.d.	N/A	**+/-**	-	0	N/A	0	N/A	N/A	N/A	0	N/A	N/A	N/A	0	0
P15	M	81	82	11	♦	Somnolence	Old left-sided infarction of the frontal and parital lobe	No IR for SARS-CoV S protein	Positive signal in mucosal cells	**+/+**	-	N/A	0	N/A	N/A	6,4*	8*	2,89	N/A	N/A	2,17	N/A	0
P16	M	74	40	51	✓	Intraventricular hemorrhage	Acute/ subacute hypoxic-ischemic encephalopathy	N/A	N/A	**+/-**	-	0	0	0	N/A	0	3,21	0	N/A	N/A	0	0	0
P17	M	70	116	51	✓	n.d.	Without significant microscopic structural changes	N/A	N/A	**+/+**	-	0	3,16	2,12	N/A	0	3,04	0	N/A	N/A	0	0	0
P18	F	30	38	21	✓	n.d.	Left temporal subarachnoid hemorrhage, cerebral toxoplasmosis with lesions in the basal ganglia and cerebellum	N/A	N/A	**+/+**	-	0	0	0,8	N/A	0	0	0	N/A	N/A	0	0	0
P19	M	77	53	51	✓	n.d., critical illness polyneuropathy	Without significant microscopic structural changes	N/A	N/A	**+/-**	-	0	0	0	N/A	0	0	0	N/A	N/A	0	0	0
P20	M	57	46	59	✓	n.d.	Without significant microscopic structural changes	IR for SARS-CoV S protein in olfactory mucosal cells and endothelial cells in the cerebellum	No signal	**+/+**	-	0	0	0	N/A	0	1,66	0	N/A	N/A	0	0	1,51
P21	M	79	168	N/A	♦	n.d.	N/A	N/A	N/A	N/A	N/A	N/A	N/A	N/A	N/A	1,29	0	0	N/A	N/A	N/A	0	0

Case	Gender	Age [years]	PMI [hours]	Duration of illness [days]	Mechanical ventilation	Neurological alterations during COVID-19 infection	CNS findings					log_{10}SARS-COV-2-RNA copies/10.000 cells											
							Histopathological	SARS-CoV S protein immunohistochemistry / Immunofluorescence (SARS CoV S protein/Tuj1)	ISH	Microglia activation/ - nodules	CD45	Carotis	Cornea	Conjunctiva	Optic nerve	Uvula	Olfactory mucosa	Olfactory bulb	Olfactory tract	Olfactory tubercle	Trigeminal ganglion	Medulla oblongata	Cerebellum
P22	M	69	94	49	✓	Striatocapsular infarction, behavioral changes, confusion, aphasia, ataxia, inabilty to walk, urinary incontinence, negative myoclonus	Without significant microscopic changes	IR for SARS-CoV S protein in corneal epithelium	No signal	N/A	N/A	0	2,6	0	N/A	0	1,9	0	N/A	N/A	0	0	0
P23	M	89	22	14	♦	n.d.	Without significant macroscopic structural changes	IR for SARS-CoV S protein in olfactory mucosal cells	N/A	**+/+**	-	0	0	0	N/A	2,64	3,85	0	N/A	N/A	0	0	0
P24	M	74	216	35	✓	N/A	Without significant macroscopic structural changes	N/A	N/A	**+/+**	-	1,8	0	0	N/A	N/A	2,54	0	N/A	N/A	0	0	0
P25	M	72	3	79	✓	n.d., critical illness polyneuropathy	Without significant microscopic structural changes	N/A	N/A	**+/+**	-	N/A	N/A	N/A	N/A	0	0	0	N/A	N/A	0	0	0
P26	F	45	48	19	✓	Headache, limb pain	Acute thalamic infarction	IR for SARS-CoV S protein in endothelial cells in infarct area	N/A	-	-	N/A	N/A	N/A	N/A	N/A	1,55	0	N/A	N/A	N/A	0	0
P27	M	71	11	N/A	n.d.	n.d.	N/A	IR for SARS-CoV S protein **IR for SARS-CoV S protein in olfactory neuronal cells**	N/A	N/A	N/A	N/A	N/A	N/A	N/A	N/A	N/A	N/A	N/A	N/A	N/A	N/A	N/A
P28	M	80	72	30	n.d.	n.d.	N/A	IR for SARS-CoV-S protein in olfactory mucosal cells	N/A	N/A	N/A	N/A	N/A	N/A	N/A	N/A	0	0	0	0	N/A	0	N/A
P29	F	72	<24	N/A	n.d.	n.d.	N/A	IR for SARS-CoV S protein in olfactory mucosal cells	No signal	N/A	N/A	N/A	N/A	N/A	N/A	N/A	3,7	0	3,1	3,2	N/A	0	N/A
P30	F	98	96	4	n.d.	n.d.	Old left middle cerebral artery infarct	IR for SARS-CoV S protein in olfactory mucosal cells, **IR for SARS-CoV S protein in olfactory neuronal cells**	No signal	N/A	N/A	N/A	N/A	N/A	0	N/A	2,15	0	0	0	N/A	3,43	N/A
P31	M	68	20	35	n.d.	n.d.	N/A	No IR for SARS-CoV S protein	No signal	N/A	N/A	N/A	N/A	N/A	3,58	N/A	1,99	0	0	0	N/A	0	N/A
P32	M	68	24	58	n.d.	n.d.	N/A	IR for SARS-CoV S protein in olfactory mucosal cells; **IR for SARS-CoV S protein in olfactory neuronal cells**	N/A	N/A	N/A	N/A	N/A	N/A	0	N/A	3,6	0	0	0	N/A	0	N/A
P33	M	63	8	29	♦	n.d.	Without significant macroscopic structural changes	No IR for SARS-CoV S protein	N/A	**+/+**	-	0	0	0	N/A	0	3,4	0	N/A	N/A	0	4,4	4,1
C1	F	63	18	N/A	✓	N/A	ALS-TDP	N/A	N/A	-	-	N/A	N/A	N/A	N/A	N/A	N/A	N/A	N/A	N/A	N/A	N/A	N/A
C2	F	62	8	N/A	♦	N/A	ALS-TDP	N/A	N/A	-	-	N/A	N/A	N/A	N/A	N/A	N/A	N/A	N/A	N/A	N/A	N/A	N/A
C3	F	84	13	N/A	♦	N/A	TDP-ALS-FTD, Alzheimers dementia, alpha-Synucleinopathy	N/A	N/A	**+/-**	-	N/A	N/A	N/A	N/A	N/A	N/A	N/A	N/A	N/A	N/A	N/A	N/A
C4	M	76	49	N/A	♦	N/A	ALS-TDP	N/A	N/A	-	-	N/A	N/A	N/A	N/A	N/A	N/A	N/A	N/A	N/A	N/A	N/A	N/A
C5	M	81	30	N/A	n.d.	N/A	Subacute pontine infarction	No IR for SARS-CoV S protein	No signal	**+/-**	-	0	0	0	N/A	0	0	0	0	0	0	0	0
C6	F	45	30	N/A	n.d.	N/A	Without significant macroscopic changes	**No IR for SARS-CoV S protein**	N/A	N/A	N/A	N/A	N/A	N/A	N/A	N/A	N/A	N/A	N/A	N/A	N/A	N/A	N/A
C7	F	86	19	N/A	♦	N/A	ALS-TDP	IR for SARS-Cov S protein in endothelial cells in the medulla oblongata	N/A	-	-	N/A	N/A	N/A	N/A	N/A	N/A	N/A	N/A	N/A	N/A	N/A	N/A
C8	M	61	168	N/A	n.d.	N/A	Alzheimer's disease - Cerebral amyloid angiopathy	**No IR for SARS-CoV S protein**	N/A	N/A	N/A	N/A	N/A	N/A	N/A	N/A	N/A	N/A	N/A	N/A	N/A	N/A	N/A
C9	F	78	144	N/A	n.d.	N/A	Macroscopic autolytic changes	No IR for SARS-CoV S protein	N/A	N/A	N/A	N/A	N/A	N/A	N/A	N/A	N/A	N/A	N/A	N/A	N/A	N/A	N/A

Case	Gender	Age [years]	PMI [hours]	Duration of illness [days]	Mechanical ventilation	Neurological alterations during COVID-19 infection	CNS findings					log$_{10}$SARS-COV-2-RNA copies/10.000 cells											
							Histopathological	SARS-CoV S protein immunohistochemistry / Immunofluorescence (SARS CoV S protein/Tuj1)	ISH	Microglia activation/ - nodules	CD45	Carotis	Cornea	Conjunctiva	Optic nerve	Uvula	Olfactory mucosa	Olfactory bulb	Olfactory tract	Olfactory tubercle	Trigeminal ganglion	Medulla oblongata	Cerebellum
C10	F	68	N/A	N/A	n.d.	N/A	N/A	No IR for SARS-CoV S protein	N/A	N/A	N/A	N/A	N/A	N/A	N/A	N/A	N/A	N/A	N/A	N/A	N/A	N/A	N/A
C11	F	27	n.d.	N/A	n.d.	N/A	N/A	**No IR for SARS-CoV S protein**	N/A	N/A	N/A	N/A	N/A	N/A	N/A	N/A	N/A	N/A	N/A	N/A	N/A	N/A	N/A
C12	M	39	N/A	N/A	n.d.	N/A	HIV-Encephalitis	N/A	N/A	**+/+**	**+**	N/A	N/A	N/A	N/A	N/A	N/A	N/A	N/A	N/A	N/A	N/A	N/A
C13	F	58	N/A	N/A	n.d.	N/A	Without significant microscopic changes	N/A	N/A	**+/-**	**-**	N/A	N/A	N/A	N/A	N/A	N/A	N/A	N/A	N/A	N/A	N/A	N/A

✓ = yes ♦ = no life-sustaining measures incl. ventilation based on patient's provision

n.d. = not documented N/A= not available IR= immunoreactivity ISH= *in situ* hybridization

= negative = positive *subgenomic RNA positive